AIRDOS – open-source PIN diode airborne dosimeter

M. Kákona,[a,b,*] J. Šlegl,[a,b] D. Kyselová,[a,b] M. Sommer,[a,b] J. Kákona,[c] M. Lužová,[a,b] V. Štěpán,[a] O. Ploc,[a] S. Kodaira,[d] J. Chroust,[e] D. John,[b] I. Ambrožová[a] and P. Krist[a]

[a] *Nuclear Physics Institute of the Czech Academy of Sciences, Husinec - Řež 130, 250 68 Řež, Cech Republic*

[b] *Czech Technical University in Prague, Faculty of Nuclear Sciences and Physical Engineering, Břehová 7, 115 19 Prague, Czech Republic*

[c] *Czech Technical University in Prague, Faculty of Electrical Engineering, Technická 2, 166 27 Prague, Czech Republic*

[d] *National Institutes for Quantum and Radiological Science and Technology, 4-9-1 Anagawa, Inage-ku, Chiba 263-8555, Japan*

[e] *Universal Scientific Technologies, Soběslav, Czech Republic*

E-mail: martin.kakona@odz.ujf.cas.cz

ABSTRACT: This article introduces a new open-source dosimeter AIRDOS intended for measurements on board aircraft. In-flight measurement of a mixed radiation field is a challenging deal that requires a small low-power-consumption battery-operated lightweight device with long endurance. A new innovative electronic design with a silicon PIN diode used as a sensor is presented, including full description and manufacturing documentation. The device was verified by measurements and compared with reference dosimeters widely used in aircraft dosimetry, such as Liulin MDU and HAWK TEPC. A comparison of the measurements with a computation model CARI 7 was performed as well. All the comparisons yield positive results within known errors. The new design of the dosimeter has a very satisfactory performance in terms of battery life and does not need calibration after manufacturing or recalibration after a long time of usage. Open-source design predetermines AIRDOS for future improvements and open-science.

KEYWORDS: PIN diode dosimeter; silicon diode dosimeter; airborne dosimeter; dosimetry on board aircraft.

* Corresponding author.

Contents

1. Introduction

Our group has been performing routine measurements of ionizing radiation on board aircraft by silicon-diode-based dosimeter Liulin since 2001 [1]. These measurements were compared with the measurements of secondary cosmic rays performed on the ground by neutron monitors [2] and with a model of secondary cosmic rays CARI [3] which is used for the estimation of aircrew doses in the Czech Republic [4]. Our effort in long-term measurements [5] has resulted in the development of a new dosimeter with a fully open design which is described here. Our motivation was the comprehension of mechanisms inside dosimeter electronics. Because in the last years many people have been spending a lot of effort on redesigning a silicon dosimeter from scratch [6-9], our aim is to introduce a fully documented open-source design which can be used as a base platform for the future improvements and modifications for the desired deployment. This newly developed airborne dosimeter, AIRDOS, has comparable properties to Liulin dosimeter [10], which enables the continuation of our long-term measurements on board aircraft and introduces new features such as calibration stability and long battery operation.

The AIRDOS is intended for measurements in low-intensity mixed ionizing radiation fields. In its aircraft version, it houses a silicon PIN diode as a radiation detector, electronics for the conversion of the signal to the pulse-height spectra, a GPS module (optional), a data logger, a memory card and batteries sufficient for up to six months of uninterrupted operation. It is a portable device for routine measurements on board aircraft. This design is built on an Open Hardware modular platform MLAB, the firmware is written in Open Software Processing

platform and data processing is written in Python using Open Software scientific libraries. Manufacturing documentation, firmware documentation and scripts for data evaluation for this dosimeter are publicly available at GitHub server [11,12].

We demonstrate the performance of AIRDOS on an example of in situ measurement on board an aircraft but the main aim of this article is to summarise the AIRDOS design and provide relevant links to the open-source technical documentation.

2. AIRDOS design

2.1 Hardware design

AIRDOS is a low-power-consumption battery-operated absorbed-dose-in-silicon spectrometer. It contains a silicon PIN diode (Hamamatsu S2744-09) [13], which serves as a sensor, analogue signal processing electronics and an acquisition unit with a data logger. Optionally, a GPS (Global Positioning System) receiver is mounted. Two LS33600 (Li-SOCl2) [14] cells are used as a power source. The endurance of the device is six months of continuous measurement without the use of GPS and one month while using GPS. The data are stored on a SD card (Secure Digital Memory Card). Block schematic of AIRDOS is depicted in figure 1 and a typical outfit with an aluminium case is shown in figure 2. Electronics are divided into two, respectively three PCB's (Printed Circuits Boards): analogue electronics (PCRD04B) [15], the GPS receiver (GPS01B) [16] and a datalogger (DATALOGGER01A) [17], see figure 3. The dosimeter modules have become a part of an open-hardware project MLAB [18]. All modules are available under the GNU General Public License v3.0 [19]. The modularity of AIRDOS allows further development, easy adding of new features, simple adding of new sensors and cooperation with the open-hardware projects.

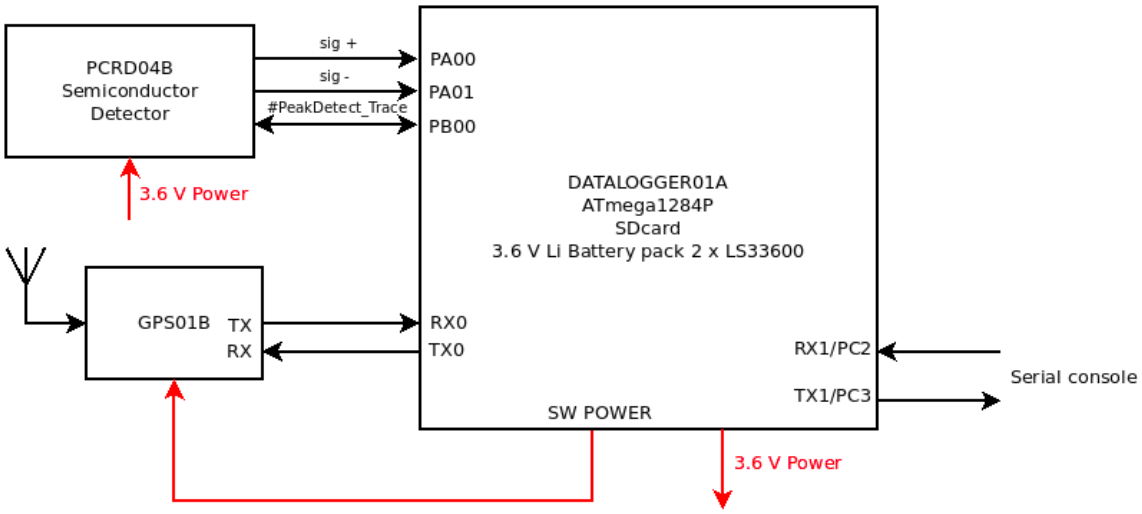

Figure 1. Block diagram of AIRDOS 02.

Figure 2. Outfit of AIRDOS 02 dosimeter.

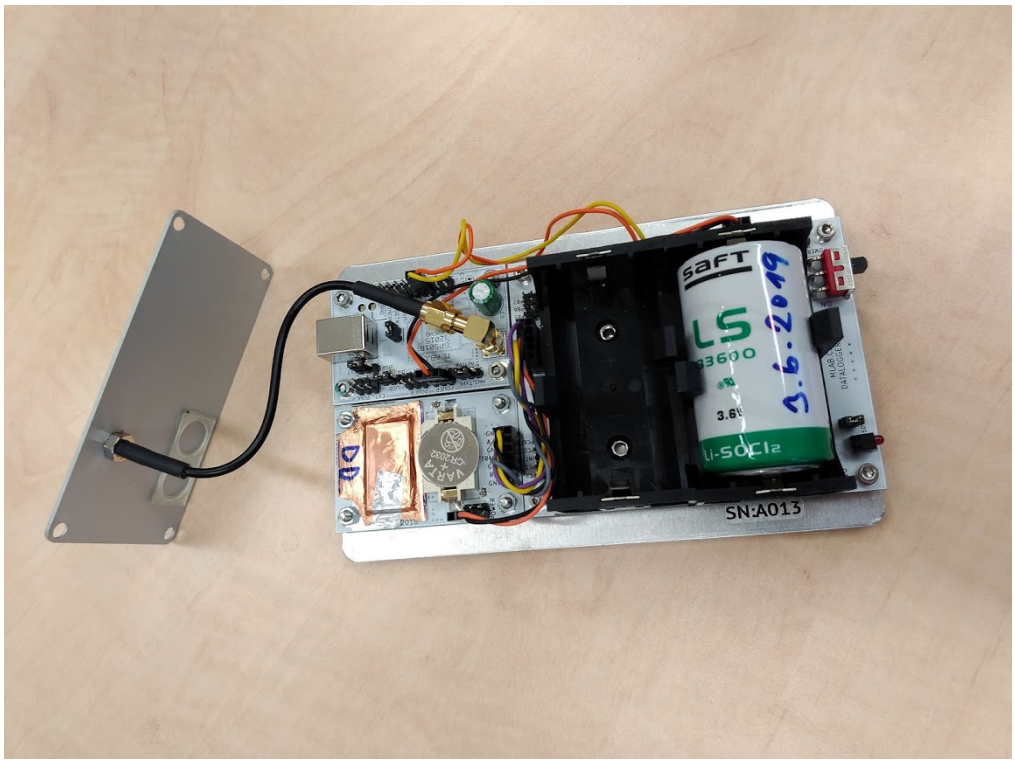

Figure 3. Deployment of PCB's inside the AIRDOS 02 dosimeter. In centre down is the analogue frontend with a PIN diode sensor covered by a copper sheet and a V_{bias} battery CR2032. Module with connected coaxial cable is the GPS.

2.2 Analog circuit design

All analogue circuits are implemented on PCB PCRD04B. Manufacturing documentation for this module is available on-line [15].

A silicon PIN photodiode (D2) is connected to a trans-impedance amplifier (figure 4) and is negatively biased by lithium cell CR2032 (BT1) with 3 V against the reference voltage REF 1.2 V.

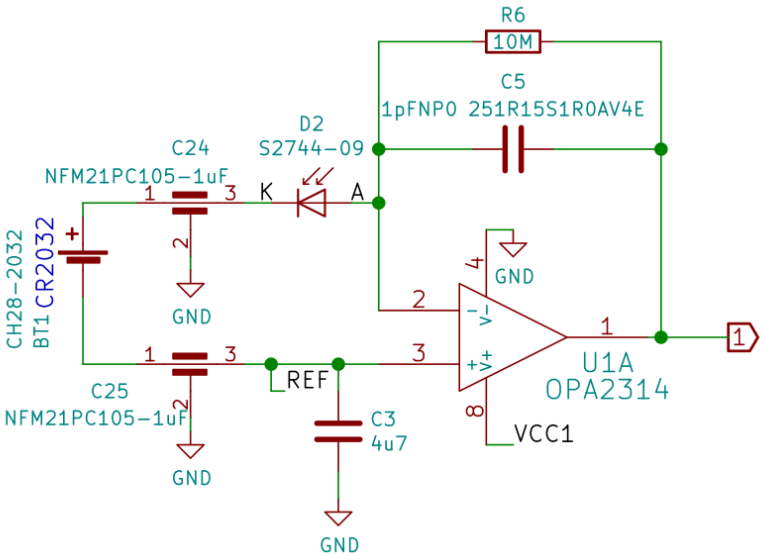

Figure 4. Silicon PIN diode sensor and charge amplifier / trans-impedance amplifier.

The voltage signal from the trans-impedance amplifier output (1) is filtered by a bandpass filter. For more information, see [15]. Each ionizing radiation event in the photodiode produces, after filtering/shaping, a pulse with a duration of about 80 µs. The amplitude of the pulse is proportional to charge in case of a constant charge collection time and the charge is proportional to the deposited energy in a sensitive volume in the PIN diode.

Resulting pulses are stored in a specially developed sample-hold circuit that behaves like a signal follower and analogue memory (figure 5). When the signal #PeakDetect_Trace is in H (high logic level) the analogue switch U5 turns on and a signal at the output U2B follows a signal at the input (2) with a slight delay which is done by the resistor R13 and the capacitor C19. If the signal #PeakDetect_Trace is switched to Z (high impedance state) the analogue switch U5 starts to be controlled by the comparator U4. In this case, when an input signal (2) goes from high to low, the positive input of the comparator will be at a higher voltage than the negative input, following a voltage at the capacitor C19. It causes switching off of the analogue switch U5 and the capacitor C19 holds its last voltage value. This behaviour is similar to a peak detector circuit. Next, the stored voltage can be converted by an ADC (Analogue to Digital Converter) and after this conversion, the input #PeakDetect_Trace goes again from Z to H and circuit changes behaviour to a signal follower circuit. The described sample-hold circuit does not suffer from typical peak detector circuits disadvantages such as insensitivity to small signals, mistreatment of negative signals or discharging the capacitor by leakage current through diodes. Moreover, this circuit can be used as a pulse discriminator as well. The signal

#PeakDetect_Trace can be connected to an input of digital circuits when it is controlled by the comparator U4. When an input signal (2) goes from high to low, the signal #PeakDetect_Trace goes from H to L (low logic level) as well. This behaviour can be used for detection of a falling edge of a signal. There is only one constraint of this circuit, the input signal can not change raising/falling time widely and an RC time constant (R13, C19) must be chosen correctly, respecting the input signal time properties.

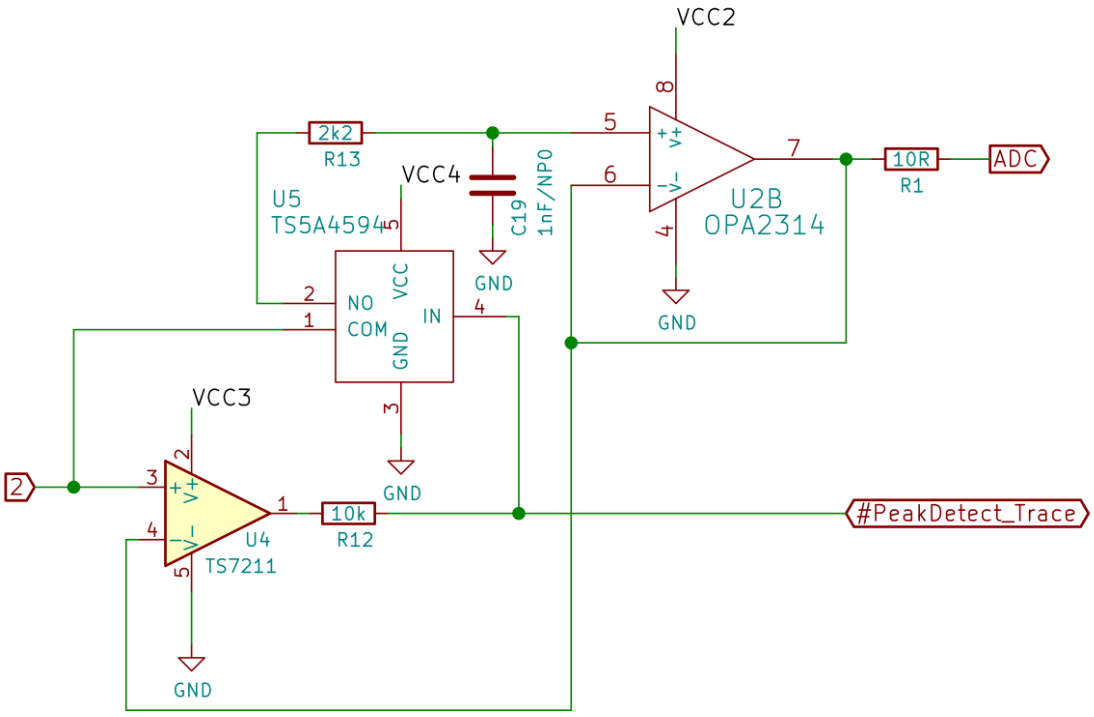

Figure 5. Signal follower with analogue memory. It is a circuit equivalent to a sample-hold circuit triggered by a falling edge of signal or a circuit equivalent to a peak detector.

2.3 Digital circuit design

A data acquisition unit is based on DATALOGGER01A module. Manufacturing documentation for this module is available on-line [17]. ATmega 1284P [20] a single chip µC (microcomputer) was used. This µC is a low power variant of ATmega 1284 and utilises a differential 10-bit ADC. Power consumption of this µC is less than 1 mA on working frequency 1 MHz (AIRDOS does not use an external crystal oscillator). Each manufactured AIRDOS contains a silicon serial number. This serial number is used as a marker for output data and helps registration of deployment of dosimeters and data pairing with specific aircraft.

The rest of the electronics comprise an RTC (Real Time Clock) with an accuracy of 20 ppm and a power switch for switching off the GPS and an SD card slot. The power supply to the SD card and the GPS is controlled by the firmware and is shut off during the dosimeter integration.

2.4 AIRDOS Firmware design

The firmware of AIRDOS was written in the Processing language environment [21] for ease of modification by non-programmers (e.g. scientists). Source code of the firmware is available under the GNU General Public License v3.0 on GitHub [22].

There is no signal discriminator in AIRDOS hardware. Consequently, AIRDOS firmware periodically samples the analogue signal. This sampling is asynchronous with ionization events and one event can accidentally belong to two neighbouring samples. This circumstance has to be solved by a software filter. Filtering algorithm is described in figure 6. This algorithm is looking for local maxima of signal and stores these local maxima to an array Histogram[].

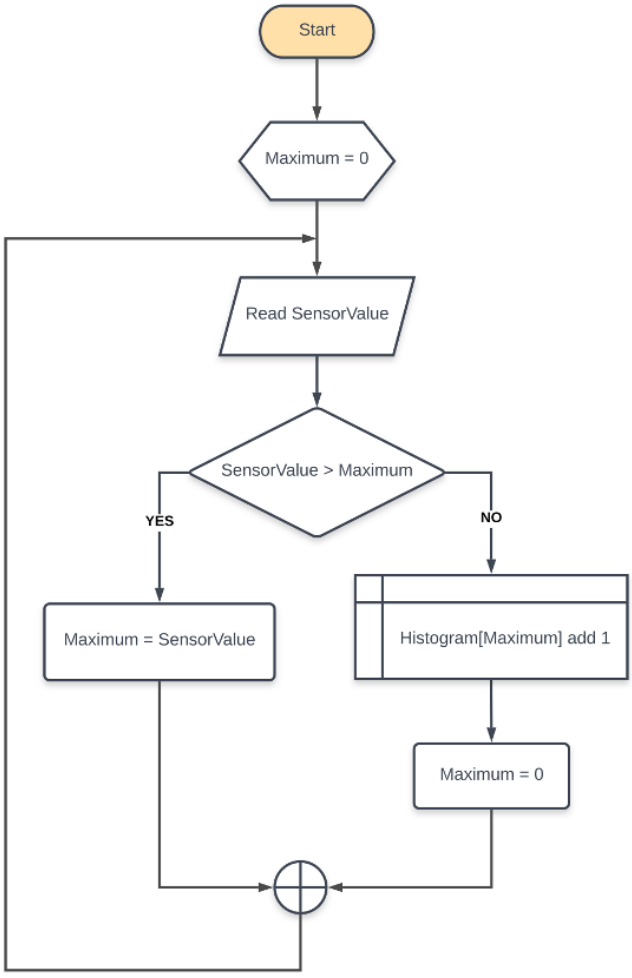

Figure 6. Flowchart of the algorithm for suppressing a double detection of events. SensorValue is a value obtained from an ADC. Maximum is a local variable. Histogram variable is an array for output values sorted by deposited energy (in channels).

2.5 AIRDOS Output

Data from AIRDOS can be obtained by an asynchronous serial protocol at UART (Universal Asynchronous Receiver/Transmitter) interface or can be stored on the SD card. The data format is described in the protocol documentation at [23]. Parsers for output data are also available as an open-source code at [24].

3. AIRDOS Calibration

3.1 Energy calibration

Energy response was investigated using a defined charge injected through a calibrated capacitor 1 ± 0.005 pF (C_T) connected to a signal generator (figure 7).

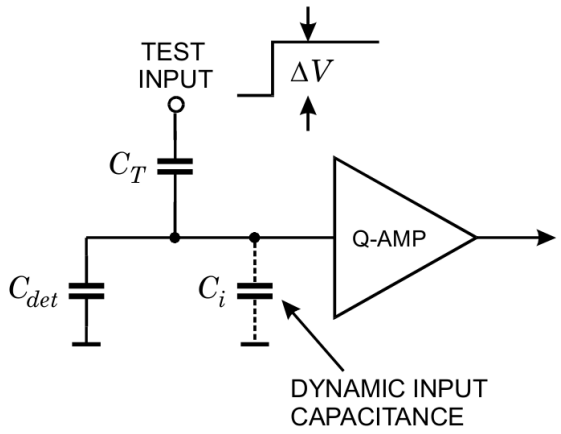

Figure 7. Circuit for calibration [25].

The slope of the rising edge of generated pulses was set to be equal to real pulses from ionisation events. The amplitude of voltage pulses (ΔV) was measured by an oscilloscope and charge was calculated using a formula

$$Q = \Delta V C_T$$

where Q is charge in Coulombs, C_T is capacity in Farads and ΔV is voltage in Volts. This formula is true in case $C_i >> C_T$. The capacity of photodiode C_{det} is two orders higher than our 1 pF capacitor (C_T) - therefore, in our case, this condition is fulfilled.

Now we can easily calculate the number of electrons corresponding to injected charge.

$$N_e = \frac{Q}{e}$$

where N_e is the number of electrons, Q is charge and e is the elementary charge (1.602×10^{-19} C).

Then, the estimated ionisation energy corresponds to the number of electron-hole pairs

$$E = N_e \varepsilon_{e-h}$$

where E is the energy in eV deposited by ionising radiation, N_e is the number of released electrons and $\varepsilon_{e\text{-}h}$ is equal to 3.65 eV for silicon [26] and it represents mean energy for electron-hole pair creation [27].

Figure 8 shows the result of energy calibration by injected charge. As can be seen, the response is perfectly linear.

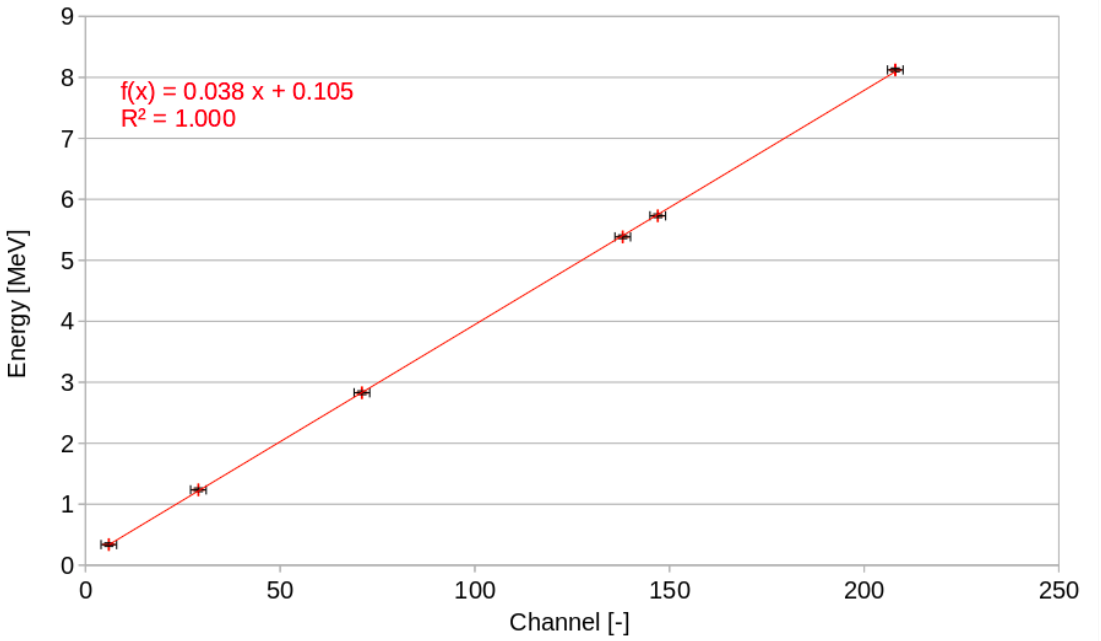

Figure 8. Energy response obtained by injecting a defined charge into the input of the charge amplifier. Depicted error bars display quantization error of the ADC.

The second method of energetic calibration is a measurement of response to real ionising particles originating in radioactive nuclides or particle accelerators. Summary of ions used for the calibration is in table 1.

Alpha particles from radionuclide sources representing heavy ion particles and protons and alpha particles from accelerators representing particles with weak interaction with the sensor were used for energy calibration of AIRDOS. This selection covers almost all the detector's energy range (from 0.2 MeV to 9 MeV). Deposited energies were calculated by SRIM program [28, 29]. Figure 9 presents responses for alpha particles from radionuclide sources (^{239}Pu, ^{241}Am), alpha particles from HIMAC (Heavy Ion Medical Accelerator in Chiba) accelerator [30] and protons from U-120M accelerator [31]. From this figure, it can be seen that measured energies from real particles slightly differ from the method of injected charge presented above. It should be noted that the real particles have to give theoretically lower values because of energy loss in an entrance window of the detector, limited lifetime of charge carriers and slower charge collection speed. However, we observed a positive offset which can be attributed to the noise of the detector. This noise is caused mainly by a current noise of the input of the trans-impedance amplifier and thermal noise/dark current of the diode. This noise is proportional to the internal capacity of the photodiode and is negligible in case of charge injected by capacitor because the capacity of the sensor is two orders higher than the capacity of the capacitor used for injecting charge.

Four manufactured AIRDOS dosimeters were checked by the method of injected charge through a capacitor, the differences in calibration between individual units are less than one channel of the ADC. We can conclude that the calibration of individual devices is not necessary.

Table 1. Table of ions used for AIRDOS energy calibration.

Source name	**Origin**	**Calculated Deposited Energy in 300 µm of Si [MeV]**
He150	HIMAC Helium 150 MeV/u	1.3
He150 + BF 1	HIMAC Helium 150 MeV/u with filter equivalent to 127.68 mm H_2O	2.8
He150 + BF 2	HIMAC Helium 150 MeV/u with filter equivalent to 142.02 mm H_2O	4.7
p+	U-120M Protons 35 MeV (31 MeV in place of detector)	1.0
p+ (3 + 4)	U-120M Protons 35 MeV with Al filters (3.14 mm of Al and 2000 mm of air)	1.7
Pu	Calibration alpha source EA14 AMPU 14 with ^{239}Pu and ^{241}Am	5.2
Am	Calibration alpha source EA14 AMPU 14 with ^{239}Pu and ^{241}Am	5.5

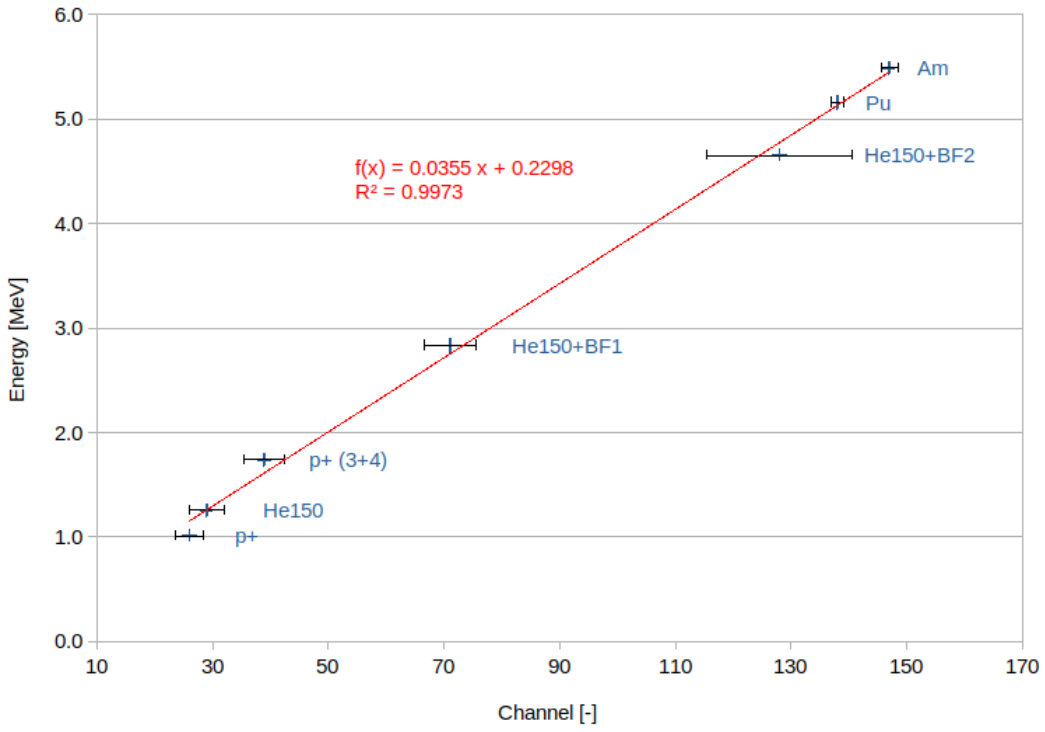

Figure 9. Energetic calibration of AIRDOS. Depicted errors are FWHM values. Used ions are described in table 1.

3.2 Thermal stability

The thermal stability of AIRDOS was tested with alpha particles from ^{241}Am and ^{239}Pu radionuclide thin layer calibration sources by cooling in the refrigerator in the temperature range from +20 °C to -15 °C. The temperature difference resulted the difference in detected deposited energy in the scale of one channel (38 keV) per 12 °C. This temperature dependence is negligible for the intended use of the detector aboard an air-conditioned commercial aircraft.

3.3 Flux calibration

AIRDOS dosimeter detects all particles up to the flux that does not cause pile-ups. Since AIRDOS is intended for use on board aircraft where the fluxes are very low with respect to the used diode area, the pile-ups are very rare. Therefore, the calibration to the flux is not needed. Only dead time must be taken into account. There are two types of dead time in AIRDOS, time for writing data to the SD card and time for obtaining absolute time and position information from the GPS. These periods should vary slightly depending on a GPS signal quality or internal file system conditions of the SD card. Nevertheless, the integration time of one measurement cycle (time for collecting data to histogram before writing to the SD card) is constant and is specifically 10.4 s. The ADC performs 46000 samples during this period. Timeout for waiting for the GPS signal is 58 s. Time for writing to the SD card alternates from 2 to 4 s depending on the SD card type and condition. We can conclude that the number of events/particles in one measurement cycle must be divided by 10.4 s to obtain the rate per second. The time needed for writing to the SD card and for obtaining position for the GPS is, in fact, dummy time without measurement and can not be calculated to the output rates.

When we want to obtain cumulative dose in silicon D_{Si}, we have to use the equation

$$D_{Si} = \frac{t_{meas}}{10.4n} \sum_{i=1}^{n} d_i$$

when d_i is a dose measured during one integration period recorded in the device datalog, t_{meas} is time of the whole measurement performed by AIRDOS in seconds and n is the number of measurements performed during the measurement period t_{meas}.

4. Results

Finally reached parameters of the design of AIRDOS are summarised in table 2. Compared to parameters of Liulin dosimeter [7] AIRDOS does not need calibration after manufacturing and there is no problem with first energy channels, because of different analogue circuits design and omitting the comparator (signal discriminator). These new features were proven by measurements described below. The last feature is the increase in operation time on batteries more than twice.

Table 2. Parameters of AIRDOS dosimeter (for version 02 F).

Dimensions	166 x 107 x 57 mm^3
Weight	730 g
Energy range	from 0.2 to 9 MeV
Number of channels	240
Channel width	38 keV
Integration time	10.4 s
Continuous measurement	6 months
PIN diode type	Hamamatsu S2744-09
Battery	2x LS 33600
Memory	SD card

Results obtained with AIRDOS were compared with Liulin dosimeter [7] in selected flight and long term measurement at high mountain observatory [32]. Differences in cumulative dose in silicon measured by Liulin and AIRDOS during the whole measurement campaign were below 10 % with systematic error +4.8 % [32]. Please note that this comparison was done for deposited energies above 250 keV. It is due to different designs of Liulin and AIRDOS dosimeters because Liulin dosimeter uses a signal discriminator/comparator which introduces jitter to first channels (lower energies) and different pieces of Liulin show different settings of the comparison level. Therefore these channels were omitted in comparison.

For assessment of radiation exposure on board aircraft measured by AIRDOS, the flight from Prague (PRG; Cutoff Rigidity = 3.5 GV) to Malaga (AGP; Cutoff Rigidity = 8.6 GV) and back was chosen. Measurement campaign lasted from 2019-11-28 16:00 to 2019-11-29 01:10 UTC and for calculation of dose time from 2019-11-28 18:55 to 2019-11-28 20:55 was used for the flight PRG-AGP and from 2019-11-28 23:00 to 2019-11-29 00:30 for the flight AGP-PRG when the aircraft was at nominal flight level. The data from three different AIRDOS devices (with serial numbers 16, 21 and F0) were used.

Calculation of an effective dose during the flight was done by CARI 7 computer program [3]]. CARI 7 uses a database of atmospheric response which is generated by Monte Carlo particle transport program MCNPX 2.7.0. Modulation of cosmic rays by the solar wind is taken into account by the monthly averages of the heliospheric potential available at FAA (Federal Aviation Administration) web site [33, 34]. Since the effective dose is not a measurable quantity, an ambient dose equivalent $H^*(10)$ is introduced [35]. For calculation of an ambient

dose equivalent rate from a dose rate in silicon provided by AIRDOS, we used an approach described in [36]. This method was established for Liulin, nevertheless, AIRDOS utilises the exact same PIN diode as Liulin thus dose in silicon has to be the same. Liulin has different energy range but particles with deposited energy higher than 9 MeV are rare on board aircraft (we encountered only 9 events over the range during both flights which represents less than 3 % of ambient dose equivalent) and lower channels (with deposited energy < 200 keV) are usually omitted in Liulin data.

First, we have to calculate the dose rate in silicon

$$\frac{dD_{Si}}{dt} = \frac{\sum_{i=4}^{250} 0.038N_i + 0.105}{m_{Si}\Delta t}$$

where coefficients (0.038 MeV and 0.105 MeV) are taken from the fit in figure 8, m_{Si} is 0.1398 g [37, 38] and integration time Δt is 10.4 s. N_i is the number of events registered in channel i.

Then we apply coefficients for conversion dose in silicon to ambient dose equivalent

$$\frac{dH^*(10)}{dt} = \frac{dD_{Si}}{dt} k_{Liulin/Airdos} k_{Sv/Gy}$$

Where $k_{Liulin/Airdos}$=1.05, it represents different channel width of Liulin and AIRDOS and this systematic difference is estimated as 5 % (lowest estimation of this systematic difference is 4.8 % by [32]), $k_{Sv/Gy}$=2.45, it is a mean value of a calibration factor for Liulin by the work [36] for the geomagnetic cutoff rigidities from 3.5 to 8.6 GV. Calculated values for the three AIRDOS devices are displayed in the graphs in figure 10 for the specific flight. We can see a change of measured value corresponding to calculation during moving a plane respecting changing the flight level and travelling through regions with different geomagnetic rigidities in time (from north to south during the flight PRG-AGP and from south to north during the flight AGP-PRG).

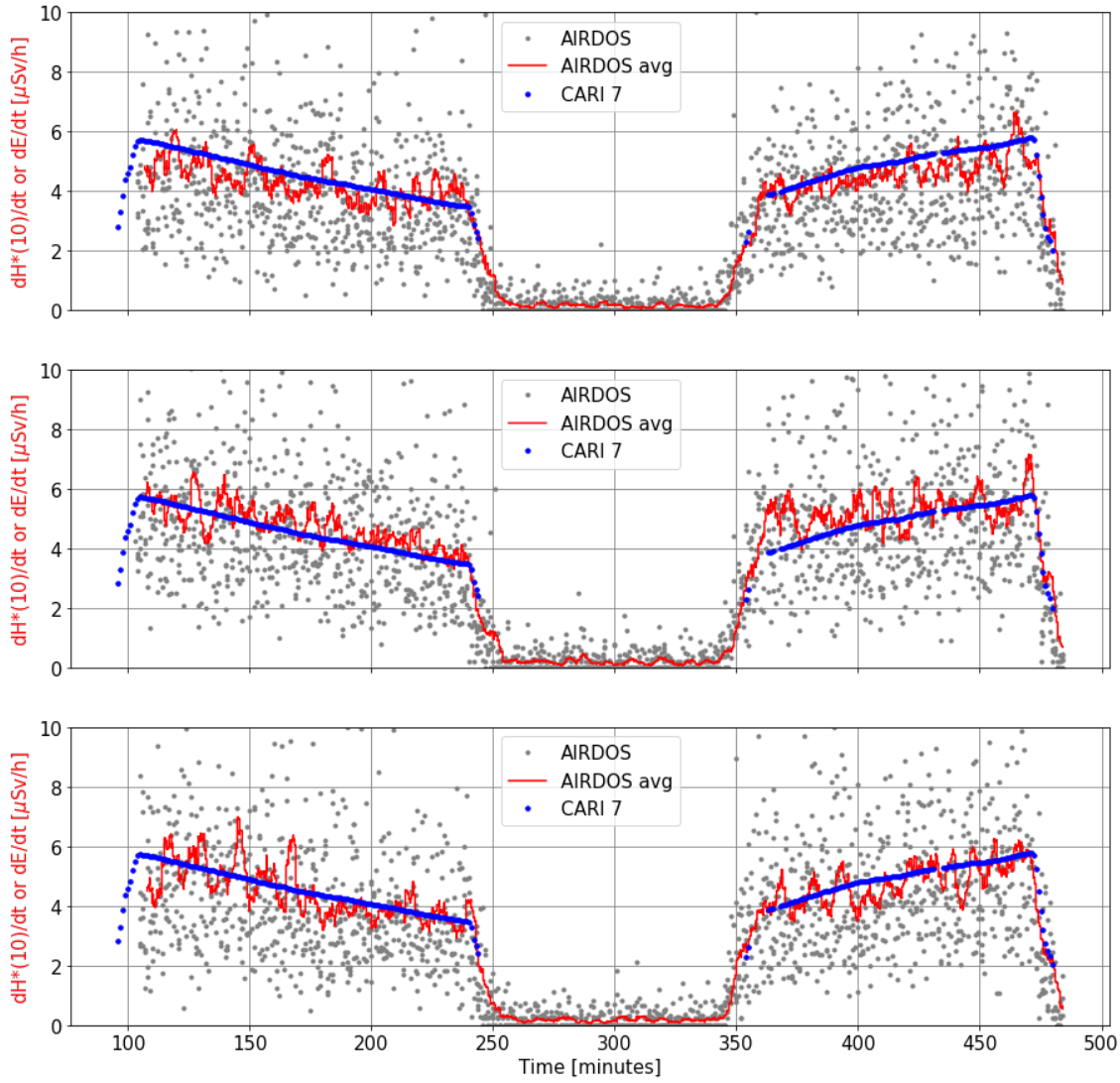

Figure 10. Radiation profiles of flights PRG-AGP (left) and AGP-PRG (right) in time. Gray points are particular measurements recalculated to ambient dose equivalent rate. Each measurement lasted 10.4 s. Red curves are running averages for 20 measurements. Blue dots are effective dose rates calculated by CARI 7 according to the flight route. Measurements were performed with AIRDOSes with serial numbers 16, 21 and F0 from the top to the bottom.

5. Discussion

In table 3, we compare the measured/calculated ambient dose equivalent (by AIRDOS) with an effective dose calculated by CARI 7. Despite the fact that the general calibration fit (from figure 8) was used and calibration for individual manufactured AIRDOSes has not been taken into account, the errors in ambient dose equivalent are mostly less than 10 %. Differences between the devices are mostly due to a DC offset of the A/D converter. This offset is compensated in the firmware but the compensation can be done with the granularity of one channel width only

(i.e. about 38 keV). This compensation is done according to chapter Offset Compensation Schemes in a datasheet [20].

Together with AIRDOSes, we performed measurement with TEPC (Tissue-Equivalent Proportional Counter) HAWK FW-AD1 dosimeter [39]. The calculated ambient dose equivalents provided by HAWK measurements are included in table 3 as well. The measured values are again within the error of 10 % compared with CARI 7 calculations which is in acceptable error by manufacturer's documentation for HAWK TEPC and by the other literature [40].

We have to add a note about the quantities used for the comparison. The effective dose E [35] provided by CARI 7 cannot be directly measured, therefore, we use the ambient dose equivalent $H^*(10)$ [35] for the AIRDOS measurements. The ambient dose equivalent is commonly used as a conservative estimation of the effective dose in the case of isotropic radiation [41]. It should also be mentioned that there are other approaches on how to determine calibration coefficients for converting D_{Si} to $H^*(10)$, for example [42].

Table 3. Comparison of doses calculated by CARI 7 program and doses measured with three manufactured dosimeters and TEPC. Please note that error of the used computation method [36] of the ambient dose equivalent is ±2.6 % and CARI 7 model deviation from ICRU reference data is from -4 % to +14 % [3]. The overall uncertainty of values provided by HAWK is 10 % [40].

	PRG-AGP		**AGP-PRG**	
Program or Dosimeter	**H*(10) or E [μSv]**	**Difference**	**H*(10) or E [μSv]**	**Difference**
CARI 7	8.7	reference value	7.6	reference value
Hawk TEPC	9.4	+8.0 %	8.1	+6.6 %
AIRDOS s.n. 16	8.8	+1.1 %	7.3	-3.9 %
AIRDOS s.n. 21	8.1	-6.9 %	6.8	-10.5 %
AIRDOS s.n. F0	9.2	+5.7 %	7.7	+1.3 %

6. Conclusions

A new open-source dosimeter for measurements on board aircraft is introduced. We tested the AIRDOS dosimeter in the real in-flight radiation field and obtained results corresponding with simulations and comparative measurements. It is the first step towards future improvements and innovations originated in the open scientific community based on a fully described open-source design. We share our effort for better understanding of solid-state dosimeters. We hope that we encourage other scientists and designers to introduce their ideas to open-science in mixed radiation field dosimetry.

Acknowledgments

I would like to thank Mikhail A. Mikhailov for providing calibrated capacitors and for guiding me through practical detector calibration.
This work was supported by EU Operational Program Research, Development, and Education in project CRREAT (CZ.02.1.01/0.0/0.0/15_003/0000481). Measurements were carried out at CANAM infrastructure of the NPI CAS Rez supported through MEYS project No. LM2015056 and at HIMAC under project H377.

References

[1] Ploc, O., Ambrozova, I., Kubancak, J., Kovar, I., & Dachev, T. P. (2013). Publicly available database of measurements with the silicon spectrometer Liulin onboard aircraft. *Radiation measurements*, *58*, 107–112. doi:10.1016/j.radmeas.2013.09.002

[2] Kákona, M., Ploc, O., Kyselová, D., Kubančák, J., Langer, R., & Kudela, K. (2016). Investigation on contribution of neutron monitor data to estimation of aviation doses. *Life Sciences in Space Research*, *11*, 24–28. doi:10.1016/j.lssr.2016.11.001

[3] Copeland, K. (2017). Cari-7a: development and validation. *Radiation Protection Dosimetry*, *175*(4), 419–431. doi:10.1093/rpd/ncw369

[4] Kubančák, J., Kyselová, D., Kovář, I., Hlaváčová, M., Langer, R., Strhársky, I., … Ploc, O. (2019). Overview of aircrew exposure to cosmic radiation in the czech republic. *Radiation Protection Dosimetry*. doi:10.1093/rpd/ncz204

[5] Kákona, M., Kyselová, D., Ambrožová, I., Kubančák, J., Štěpán, V., Langer, R., … Ploc, O. (2019). CR10 - a public database of cosmic radiation measurements at aviation altitudes of about 10 km. *Radiation Protection Dosimetry*. doi:10.1093/rpd/ncz207

[6] Dachev, T., Dimitrov, P., Tomov, B., & Matviichuk, Y. (2001). Technical Description of LIULIN-4 type LET Spectrometers (LETS) . Retrieved from http://citeseerx.ist.psu.edu/viewdoc/download?doi=10.1.1.504.2611&rep=rep1&type=pdf

[7] Dachev, T., Dimitrov, P., Tomov, B., & Matviichuk, Y. (2009). Technical Description of the Spectrometer-Dosimeter Liulin-6C MDU-6.

[8] Ritter, B., Maršálek, K., Berger, T., Burmeister, S., Reitz, G., & Heber, B. (2014). A small active dosimeter for applications in space. *Nuclear Instruments and Methods in Physics Research Section A: Accelerators, Spectrometers, Detectors and Associated Equipment*, *748*, 61–69. doi:10.1016/j.nima.2014.02.030

[9] Berger, T., Marsalek, K., Aeckerlein, J., Hauslage, J., Matthiä, D., Przybyla, B., … Wirtz, M. (2019). The German Aerospace Center M-42 radiation detector-A new development for applications in mixed radiation fields. *The Review of scientific instruments*, *90*(12), 125115. doi:10.1063/1.5122301

[10] Dachev, T., Tomov, B., Matviichuk, Y., Dimitrov, P., Lemaire, J., Gregoire, G., … Spurny, F. (2002). Calibration results obtained with Liulin-4 type dosimeters. *Advances in Space Research*, *30*(4), 917–925. doi:10.1016/S0273-1177(02)00411-8

[11] Kákona, M., Chroust, J., Kákona, J., Lužová, M., Kyselová, D., Šlegl, J., … Krist, P. (2017). AIRDOS01. Retrieved January 1, 2020, from https://github.com/ODZ-UJF-AV-CR/AIRDOS01

[12] Kákona, M., & Chroust, J. (2018). AIRDOS02. Retrieved January 1, 2020, from https://github.com/ODZ-UJF-AV-CR/AIRDOS01

[13] HAMAMATSU. (2011). PIN photodiode S2744-09. Retrieved December 9, 2019, from https://www.hamamatsu.com/resources/pdf/ssd/s2744-08_etc_kpin1049e.pdf

[14] SHAFT. (2019). LS 33600 Primary cell datasheet.

[15] Kákona, M. (2018). PCRD04B. *MLAB*. Retrieved January 1, 2020, from https://github.com/MLAB-project/Modules/tree/master/sensors/PCRD04B

[16] Chroust, J. (2015). GPS01B MLAB module. *GPS01B MLAB module*. Retrieved November 30, 2020, from https://github.com/mlab-modules/GPS01/tree/GPS01B

[17] Kákona, M., & Chroust, J. (2018). DATALOGGER01A. *MLAB*. Retrieved January 1, 2020, from https://github.com/MLAB-project/Modules/tree/master/sensors/DATALOGGER01A

[18] MLAB. (2003). MLAB project. *MLAB*. Retrieved January 8, 2020, from https://mlab.cz/

[19] GNU. (2007). GNU General Public License v. 3.0. *GNU General Public License*. Retrieved January 8, 2020, from https://www.gnu.org/licenses/gpl-3.0.en.html

[20] Microchip. (2018). ATmega164A/PA/324A/PA/644A/PA/1284/P, (ISBN: 978-1-5224-3637-9).

[21] Processing Foundation. (2001). Processing language. Retrieved January 9, 2020, from https://processing.org/

[22] Kákona, M. (2018). AIRDOS Firmware. *GitHub AIRDOS firmware*. Retrieved January 1, 2020, from https://github.com/ODZ-UJF-AV-CR/AIRDOS02/tree/AIRDOS02A/sw

[23] Kákona, M. (2019). AIRDOS data format. *GitHub AIRDOS wiki*. Retrieved January 1, 2020, from https://github.com/ODZ-UJF-AV-CR/AIRDOS01/wiki/AIRDOS-data-format

[24] Kákona, M. (2017). AIRDOS data parser. *GitHub AIRDOS parser*. Retrieved January 1, 2020, from https://github.com/ODZ-UJF-AV-CR/AIRDOS-parser

[25] Spieler, H. (2012). Silicon Detectors. *IEEE 2012 Nuclear Science Symposium, Medical Imaging Conference*.

[26] Mazziotta, M. N. (2008). Electron–hole pair creation energy and Fano factor temperature dependence in silicon. *Nuclear Instruments and Methods in Physics Research Section A: Accelerators, Spectrometers, Detectors and Associated Equipment*, *584*(2–3), 436–439. doi:10.1016/j.nima.2007.10.043

[27] Alig, R. C., & Bloom, S. (1975). Electron-Hole-Pair Creation Energies in Semiconductors. *Physical Review Letters*, *35*(22), 1522–1525. doi:10.1103/PhysRevLett.35.1522

[28] Ziegler, J. F. (2010). SRIM. Retrieved January 5, 2020, from http://www.srim.org/index.htm

[29] Ziegler, J. F., Ziegler, M. D., & Biersack, J. P. (2010). SRIM – The stopping and range of ions in matter (2010). *Nuclear Instruments and Methods in Physics Research Section B: Beam Interactions with Materials and Atoms*, *268*(11–12), 1818–1823. doi:10.1016/j.nimb.2010.02.091

[30] Yamada, S. (1995). Commissioning and performance of the HIMAC medical accelerator. In *Proceedings Particle Accelerator Conference* (pp. 9–13). Presented at the Particle Accelerator Conference, IEEE. doi:10.1109/PAC.1995.504557

[31] Křížek, F., Ferencei, J., Matlocha, T., Pospíšil, J., Príbeli, P., Raskina, V., … Vysoká, K. (2018). Irradiation setup at the U-120M cyclotron facility. *Nuclear Instruments and Methods in Physics Research Section A: Accelerators, Spectrometers, Detectors and Associated Equipment*, *894*, 87–95. doi:10.1016/j.nima.2018.03.066

[32] Kákona, M., Štěpán, V., Ambrožová, I., Arsov, T., Chroust, J., Kákona, J., … Angelov, C. (2019). Comparative measurements of mixed radiation fields using liulin and AIRDOS dosimeters (Vol. 2075, p. 130003). Presented at the 10th Jubilee International Conference of the Balkan Physical Union, Author(s). doi:10.1063/1.5091288

[33] Copeland, K., Friedberg, W., Duke, F., Snyder, L., O'Brien, K., Parker, D., … Smart, D. (2017, June 6). CARI 7. *Computer program CARI-7*. Retrieved December 8, 2019, from https://www.faa.gov/data_research/research/med_humanfacs/aeromedical/radiobiology/cari7/

[34] FAA. (2019). Heliocentric potential. Retrieved January 1, 2020, from https://www.faa.gov/data_research/research/med_humanfacs/aeromedical/radiobiology/heliocentric/

[35] ICRP. (2007). ICRP Publication 103, The 2007 Recommendations of the International Commission on Radiological Protection. *Annals of the ICRP*.

[36] Wissmann, F., & Klages, T. (2019). A simple method to monitor the dose rate of secondary cosmic radiation at altitude. *Journal of radiological protection : official journal of the Society for Radiological Protection*, *39*(1), 71–84. doi:10.1088/1361-6498/aaeeae

[37] Meier, M. M., Trompier, F., Ambrozova, I., Kubancak, J., Matthiä, D., Ploc, O., … Wirtz, M. (2016). CONCORD: comparison of cosmic radiation detectors in the radiation field at aviation altitudes. *Journal of Space Weather and Space Climate*, *6*, A24. doi:10.1051/swsc/2016017

[38] Uchihori, Y., Kitamura, H., Fujitaka, K., Dachev, T. P., Tomov, B. T., Dimitrov, P. G., & Matviichuk, Y. (2002). Analysis of the calibration results obtained with Liulin-4J spectrometer-dosimeter on protons and heavy ions. *Radiation measurements*, *35*(2), 127–134. doi:10.1016/s1350-4487(01)00286-4

[39] Far West Technology, Inc. (2010). "HAWK" TEPC ENVIRONMENTAL MONITOR MODEL FW-AD1. Retrieved January 1, 2020, from https://www.fwt.com/detector/fw-ad1ds.htm

[40] Farah, J., De Saint-Hubert, M., Mojżeszek, N., Chiriotti, S., Gryzinski, M., Ploc, O., … Olko, P. (2017). Performance tests and comparison of microdosimetric measurements with four tissue-equivalent proportional counters in scanning proton therapy. *Radiation measurements*, *96*, 42–52. doi:10.1016/j.radmeas.2016.12.005

[41] ICRU. (2010). Report 84. *Journal of the ICRU*, *10*(2), NP-NP. doi:10.1093/jicru/10.2.Report84

[42] Ploc, O., Pachnerová Brabcová, K., Spurny, F., Malušek, A., & Dachev, T. (2011). Use of energy deposition spectrometer Liulin for individual monitoring of aircrew. *Radiation Protection Dosimetry*, *144*(1–4), 611–614. doi:10.1093/rpd/ncq505